INTERFACE

royalsocietypublishing.org/journal/rsif

Research

Cite this article: Van Gorp MJW, Goyens J, Alfaro ME, Van Wassenbergh S. 2022 Keels of boxfish carapaces strongly improve stabilization against roll. *J. R. Soc. Interface* **19**: 20210942.
https://doi.org/10.1098/rsif.2021.0942

Received: 21 December 2021
Accepted: 31 March 2022

Subject Category:
Life Sciences–Physics interface

Subject Areas:
biomechanics, biophysics

Keywords:
swimming, manoeuvrability, hydrodynamics, carapace, stabilization, drag

Author for correspondence:
Merel J. W. Van Gorp
e-mail: merel.vangorp@uantwerpen.be

Electronic supplementary material is available online at https://doi.org/10.6084/m9.figshare.c.5953471.

THE ROYAL SOCIETY
PUBLISHING

Keels of boxfish carapaces strongly improve stabilization against roll

Merel J. W. Van Gorp[1], Jana Goyens[1], Michael E. Alfaro[2] and Sam Van Wassenbergh[1]

[1]Department of Biology, Universiteit Antwerpen, Universiteitsplein 1, 2610 Antwerpen, Belgium
[2]Department of Ecology and Evolutionary Biology, University of California, 2154 Terasaki Life Sciences Building, Los Angeles, CA 90095, USA

MJWVG, 0000-0002-3058-1323; JG, 0000-0003-0176-884X; SVW, 0000-0001-5746-4621

Boxfish (Ostraciidae) have peculiar body shapes, with conspicuous keels formed by their bony carapaces. Previous studies have proposed various hydrodynamic roles for these keels, including reducing drag during swimming, contributing to passive stabilization of the swimming course, or providing resistance against roll rotations. Here, we tested these hypotheses using computational fluid dynamics simulations of five species of Ostraciidae with a range of carapace shapes. The hydrodynamic performance of the original carapace surface models, obtained from laser scanning of museum specimens, was compared with models where the keels had been digitally reduced. The original carapaces showed no reduced drag or increased passive stability against pitch and yaw compared to the reduced-keel carapaces. However, consistently for all studied species, a strong increase in roll drag and roll-added mass was observed for the original carapaces compared to the reduced-keel carapaces, despite the relatively small differences in keel height. In particular, the damping of roll movement by resistive drag torques increased considerably by the presence of keels. Our results suggest that the shape of the boxfish carapace is important in enabling the observed roll-free forward swimming of boxfish and may facilitate the control of manoeuvres.

1. Introduction

Aquatic vertebrates display various morphological adaptations for life in water. To obtain a better understanding of these adaptations, it is necessary to delve into the dynamic interactions between the body and the medium without overlooking ecological aspects [1]. Aquatic habitats are characterized by the presence of non-uniformities and random disturbances in the flow field around the fish; therefore, during locomotion, the body is subjected to a large number of external forces that may throw it out of balance [1,2]. Aquatic animals can overcome these destabilizing forces through active correction using fin or body movements. Disturbances can also be damped passively, using various morphological features, such as body proportions in general or the presence of specific structures on the body [2–5].

The body of boxfish (Ostraciidae) is completely covered by a shell of fused hexagonal bony plates, known as the carapace. This rare feature is shared by all members of the Ostraciidae family, a group of 23 extant species found in the Atlantic, Indian and Pacific Oceans, generally at middle latitudes. Carapace geometry varies greatly between species [6–8] and serves as a bony armour that provides protection against bites of coral-reef-dwelling predators [9]. Boxfish have accurate control over manoeuvres, which is essential for foraging in spatially complex habitats such as coral reefs [10–13]. In fish, propulsion is usually driven largely by undulations of the body. As the rigidity of the carapace prohibits any bending of the body, boxfish depend solely on their five fins for locomotion [11,14]. This situation is similar to many rigid man-made aquatic vessels in which high movement efficiency is strongly pursued; thus, boxfish morphology has fuelled several studies of bioinspired design in aquatic engineering sciences [15–20].

A general feature of the carapace of boxfish is the presence of longitudinal ridges, the keels. In addition to the potential role of protruding ridges in anti-predator defence (together with the protection provided by the carapace as a whole) [8], boxfish carapace keels have been hypothesized to be a critical factor contributing to different hydrodynamic properties, namely, by reducing the drag coefficient (hypothesis 1, H1) [21–23], by generating stabilizing yaw and pitch torques to help the boxfish maintain straight swimming trajectories (hypothesis 2, H2) [21–23], and by providing resistance against rolling (hypothesis 3, H3) [24]. Evidence for the drag reduction hypothesis (H1) has already been found in other marine vertebrates, such as the leatherback sea turtle (*Dermochelys coriacea*), in which the longitudinal ridges suppress boundary layer separation [5]. Whether the keels of boxfish contribute to drag reduction, however, remains untested.

The hypothesis that the keels contribute to stabilizing rectilinear swimming by generating self-stabilizing yaw and pitch torques (H2) was inferred from vortical flows and pressures measured experimentally near the boxfish keels [22,23,25]. However, recent studies on two boxfish species, *Lactophrys triqueter* with a triangular body shape and *Ostracion cubicus* with a rectangular body shape, demonstrated that the overall torque by flow past the carapace under yaw and pitch angles of attack is not self-stabilizing but rather destabilizing [13,24]. Nevertheless, a role in *reducing destabilization* seems unlikely, as the destabilizing hydrodynamic properties of the carapace improve the manoeuvrability of the boxfish, and the role of the keels to reduce this effect appears to be in conflict with the ecological demands of the boxfish in terms of manoeuvrability and agility [10,12].

Lastly, the hypothesis that keels in Ostraciidae dampen roll rotations (i.e. around the rostro-caudal axis; H3) corresponds to the function of keels in boats and other engineered aquatic vehicles. In these systems, keels are ubiquitous as a passive stability system to reduce the tendency to roll [26–34]; they are also used in pairs on either side of the ship, what is known as bilge keels [26–29]. Keels provide a larger lateral plane and wetted surface area, resulting in increased hydrodynamic resistance against roll rotations [30,31,35,36].

The alleged hydrodynamic properties of boxfish in terms of drag reduction, passive stability and manoeuvrability make them an interesting subject for robotic engineers, with several prototypes of boxfish-inspired micro underwater vehicles already in existence [15–20]. As interest in autonomous underwater vehicles is expected to grow significantly in the near future, there should be more clarity concerning the hydrodynamic properties of model species for bioinspired designs. Here, we investigated whether the keels on the carapace reduce drag during forward swimming (H1), increase the stability of the carapace in pitch and yaw angles of attack (H2) or increase roll stability through increased rotational drag and/or rotational added mass about the centre of volume of the carapace (H3). This was studied across five boxfish species using a computational fluid dynamics (CFD) approach in which the scans of the original specimens were compared to 'reduced-keel models' that had the most protruding parts of the keels blunted.

2. Material and methods

2.1. 3D laser scanning of museum specimens

Not all species will benefit equally from possessing keels as keel efficiency will vary between body shapes; therefore, we selected five species to represent the diversity of carapace shape in Ostraciidae: *Acanthostracion guineensis* Bleeker, 1865 (pentagonal cross-section) from the Academy of Natural Sciences of Drexel University (accession no. ANSP 102873); smooth trunkfish *Lactophrys triqueter* Linnaeus, 1758 Jordan & Evermann, 1898 (triangular cross-section); longhorn cowfish *Lactoria cornuta* Linnaeus, 1758 (trapezoidal cross-section); yellow boxfish *Ostracion cubicus* Linnaeus, 1758 (square cross-section) from the Natural History Museum of Los Angeles County (accession nos. LACM 8088, LACM 38229, LACM 42481, respectively); and horn-nose boxfish *Rhynchostracion rhinorhynchus* Bleeker, 1852 (square cross-section) from the former Stanford University collection, now housed in California Academy of Sciences (accession no. SU 28102). Despite studying only one specimen per species, the analysed effects of interspecific variability in carapace shape on keel function will also cover the potential effects of smaller intraspecific variability. Three-dimensional surface scans were obtained by laser scanning of the preserved specimen using a NextEngine 3D scanner HD (NextEngine, Santa Monica, CA, USA). One 360° set of scans captured the body and tail, and one set of three scans at 36° offset captured the head. These scans were later merged. A clean-up of the 3D model was performed using Scanstudio software and Geomagic (v. 2017, Geomagic, Research Triangle Park, NC, USA) to remove the pectoral, dorsal and anal fin(s) and to eliminate artificial sharp edges and holes in the model when present.

2.2. Digital manipulation of the keels

Apart from these original models, the second set of carapace models was prepared in which the keels were significantly reduced in size. To do so, the sharpest part of the keels was cut out of the surface mesh, leaving holes that were subsequently filled with the curvature-based filling function of Geomagic. Standardization of the keel reduction was hampered by the interspecific variation in keel shape and sharpness. To quantify to what extent the keels had been reduced, we calculated the difference compared to the original mesh (figure 1), which, despite the variation in the strength of manipulations between species, allowed us to evaluate the pre–post effects on the different functions for each species. Lastly, we placed all carapace models with their centre of volume in the origin of a coordinate system, and their orientation was aligned with the three orthogonal axes (figure 2).

2.3. Flow domain and meshing

The boxfish carapace models were imported into Ansys Fluent with TGrid meshing (release 19.1, Ansys Inc., Canonsburg, PA, USA) in a cylinder-shaped flow domain with a radius of 0.3 m and a length of 1.9 at 0.4 m from the velocity inlet (figure 2*a*). To simulate the water surrounding the body using CFD, the partial differential equation that describes the state of the fluid was numerically solved for each partial volume of the flow domain; therefore, a mesh was constructed that divided the space into small tetrahedral partial volumes or mesh elements. To obtain a higher resolution close to the body without unnecessary high resolution far from the fish, a refinement box was constructed around the body (length = 320 mm; width and height = 120 mm; figure 2*a*). Outside the refinement box, the growth factor of the mesh elements was set at 1.1, while inside the refinement box a growth factor of 1.04 was used. This resulted in slower growth and smaller mesh elements inside the refinement box.

To validate the precision of the mesh, a mesh convergence test was performed for one of the studied boxfish (*O. cubicus*) using six meshes of increasing refinement (figure 2*c*). Drag force (using CFD settings as outlined below) differed negligibly (1.3%) between the calculation that used a mesh of 20.7 million elements (mesh edge length at boxfish = 0.1 mm) and the

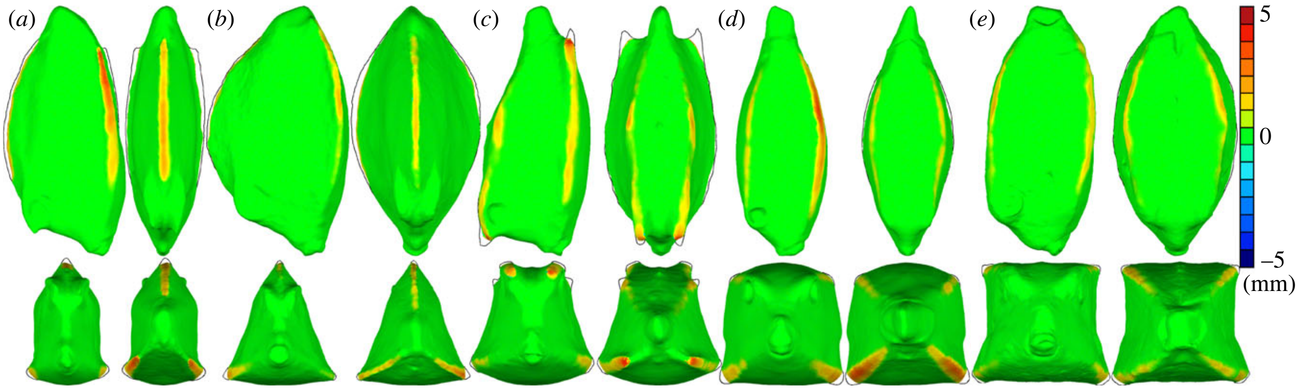

Figure 1. Deviations between the reduced-keel and original model projected on the reduced-keel model for (*a*) *Acanthostracion guineensis*, (*b*) *Lactophrys triqueter*, (*c*) *Lactoria cornuta*, (*d*) *Ostracion cubicus* and (*e*) *Rhynchostracion rhinorhynchus*. The contours of the original keels are illustrated by a black line. Maximal deviations for these models were, respectively, 3.90, 3.47, 3.30, 4.05 and 1.57 mm. Views are lateral (top left), dorsal (top right), frontal (bottom left) and posterior (bottom right).

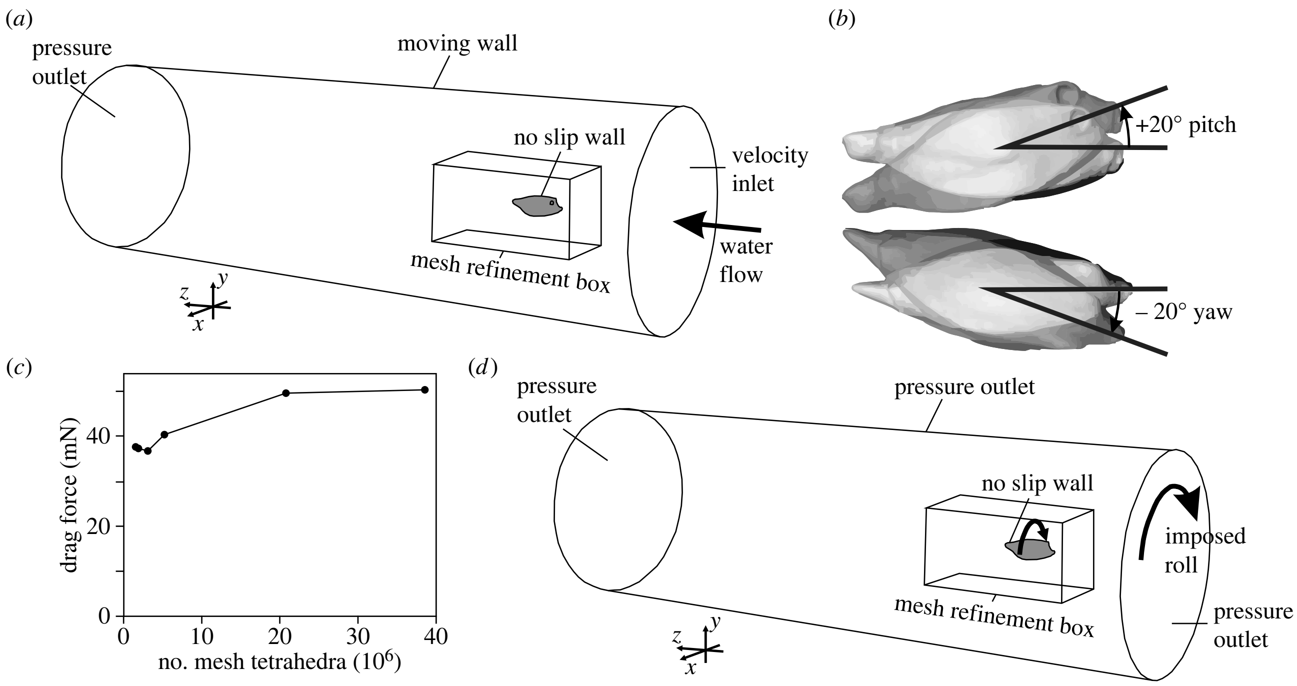

Figure 2. (*a*) Cylinder-shaped flow domain used for computational fluid dynamics, with indication of boundary conditions for drag, pitch and yaw calculations. (*b*) Overview of simulated angles of attack: +20° pitch (around the *x*-axis) to assess pitch stability, and −20° yaw (around the *y*-axis) to assess yaw stability. (*c*) Calculated drag forces of *O. cubicus* using six different meshes with the various resolution, indicating mesh convergence around 20 million mesh elements. (*d*) Flow domain and boundary conditions for imposed roll simulations. Note that in (*d*) the entire mesh is rotated, but the water remains unaffected apart from the vicinity of the boxfish where it is moved by the rotating carapace.

calculation that used a mesh of 38.5 million elements (mesh edge length at boxfish = 0.05 mm), showing that using meshes of 20.7 million elements was sufficiently accurate. Therefore, we used 20.7 million element meshes for all further calculations.

2.4. Steady-flow computational fluid dynamics

In the first type of CFD simulation, a steady water flow was simulated over a stationary boxfish carapace at different angles of attack. The boundary face in front of the boxfish was defined as a velocity inlet with a flow velocity of 0.5 m s^{-1}, which is equivalent to a fish swimming at 0.5 m s^{-1} in still water. This velocity was used in previous research and is considered the velocity of boxfish during fast swimming [22,24]. Additional simulations run at 0.1 m s^{-1} for *A. guineensis* and *O. cubicus* showed similar relative differences, indicating that the reported results at 0.5 m s^{-1} apply to slower swimming speeds as well. The boxfish carapace surface was defined as a 'wall' where the no-slip boundary condition applies. The mantle of the cylinder was modelled as a wall moving posteriorly at the same velocity as the water. The circular boundary face at the back was set as a pressure outlet with zero gauge pressure (figure 2*a*), as they were assumed too distant from the fish to encounter pressure disturbances in the flow. The fluid in the model had a water density (ρ) of 998.2 kg m^{-3} and a dynamic viscosity of 1.001 Pa s. To account for the effects of turbulence at relatively low Reynolds numbers, Menter's shear stress transport (Transition SST) model was used, which is a robust four-equation eddy-viscosity turbulence model widely used in CFD [37]. This model was previously validated against force and torque measurements in a flow tank [13,24]. Convergence was safely reached before the end of the imposed 2000 iterations. This was monitored through the scaled residues of each of the equations and by checking if the drag force evolved towards a constant solution.

2.5. Drag force, pitch and yaw stability

The drag force (H1) was determined for the models with their rostro-caudal axis parallel with the incoming water flow. As the reduced-keel models have a slightly smaller wetted and projected surface area, the dimensionless drag coefficient (C_D) (equation (2.1)) was used to assess the effect on drag by the altered shape of the carapace (by reducing the keels) independently of absolute size and swimming speed, in a certain flow regime. Both pressure drag and viscous drag are taken into account in this coefficient. To measure the (de)stabilizing pitch and yaw moments in a static set-up (H2), boxfish models were placed in a flow at a slight pitch (+ 20° around the x-axis; right-hand rule; nose-up) or yaw angle (− 20° around the y-axis), respectively (figure 2*b*). This was a representation of the boxfish no longer oriented in line with its direction of motion. When the body is inherently stable, it will automatically return to its aligned position; if not, it will rotate further away from its alignment with the water flow. The presence of a passive stabilizing mechanism can be evaluated from the CFD through the sign of rotational moments. For the orientations used in our simulations (figure 2*a*,*b*), stabilizing moments were negative for pitch, and positive for yaw (i.e. opposing the sign of the angle of attack).

Similar to the drag coefficient, to assess the effect on (de)stabilizing moments by the altered shape of the carapace independent of size and flow velocity, pitch (equation (2.2)) and yaw moment coefficients (equation (2.3)) were calculated [22,38]. The drag and moment coefficient equations were

$$C_D = \frac{2F_z}{\rho\, u^2 A_z}, \tag{2.1}$$

$$C_{\mathrm{Mpitch}} = \frac{2M_x}{\rho\, u^2 A_y\, L_z}, \tag{2.2}$$

and

$$C_{\mathrm{Myaw}} = \frac{2M_y}{\rho\, u^2 A_x\, L_z}, \tag{2.3}$$

with the drag force (F_z), pitch moment (M_x) and yaw moment (M_y) about the centre of the volume calculated by Ansys Fluent, the frontal projected area of the boxfish carapace in the direction of the flow (A_z), the dorsoventral projected area in the direction of the y-axis (A_y), the lateral projected area in the direction of the x-axis (A_x), the chord length of the body (L_z), the water density (ρ) and the velocity of the flow (u) [22,24,39,40].

2.6. Transient computational fluid dynamics of an imposed roll rotation

The resistance against roll rotation (H3) was determined by calculating the z-component of the moment as a function of time during a short period, during which we imposed a roll rotation of constant acceleration on the body of the boxfish in stagnant water. To impose such a roll rotation, a DEFINE_CG_MOTION user-defined function was used, which was assigned to the carapace, the outer boundary faces, and the interior mesh elements, but not to the fluid. This was a mathematical approach to simulate the effect of an external torque on the fish's body. In natural situations, this could be the result of variable water currents, or of the fish's fin forces during manoeuvring. Since all meshes rotated, there was no deformation of the mesh. Although a spherical domain surrounding the boxfish would be optimal to reduce computational times, to avoid having to remake the mesh, we used the same domain geometry and mesh as in the steady-flow simulations. The boundary conditions for these roll simulations (figure 2*d*) were modified compared to the steady-flow simulations (figure 2*a*): the front face, the back face and the mantle of the cylinder were set as pressure outlets (zero gauge pressure). By imposing roll rotation intrinsically rather than exposing it to an external current, the velocity vector field was easier to interpret. Over time, a rotation with constant acceleration led to a linear increase in angular velocity, and the rotated angle increased in a quadratic manner [41].

A laminar flow model was used because the simulations were of such a short duration (0.2 s) that a transition to turbulence should not occur. To simulate the course of the imposed rotation and the moments experienced in time, a transient-state simulation was used instead of a steady-state simulation. This meant that for each variable, the instantaneous value was calculated in each time step. Simulations were run for three different rotational accelerations: 20 rad s^{-2}, 40 rad s^{-2} and 80 rad s^{-2}, imposed on the carapace for a time period of 0.2 s, which resulted in a total rotation of 0.4 rad, 0.8 rad and 1.6 rad, respectively. We used 50 time steps of $\Delta t = 0.004$ s, with each time step calculated in 25 iterations. This choice was justified by a convergence test for *O. cubicus*, which showed scaled residuals to reach the standard 10^3 drop criterion. We also tested whether the time step size was sufficiently small for *O. cubicus* by comparison to a simulation with 100 time steps of $\Delta t = 0.002$ s. This simulation only resulted in a difference in the calculated moment of 0.7%, and therefore did not justify doubling the computational time. By rotating only for a very short time interval, the flow patterns were representative of small perturbations.

2.7. Roll stability assessment

Unlike resistance against forces and moments for stationary objects (equations (2.1)–(2.3)), resistance against imposed roll consisted of geometry-dependant rotational drag, as well as added mass [38,42–45]. The moment $M_z(t)$ that is needed to overcome the rotational resistance for a certain imposed rotation $\varphi(t)$, was

$$M_z(t) = -|\dot{\varphi}(t)|\ \dot{\varphi}(t)\ L_z^5\ \rho\ C_{\mathrm{rotD}} - \ddot{\varphi}\ L_z^5\ \rho\ C_{\mathrm{rotAM}}, \tag{2.4}$$

with the rotational drag moment coefficient (C_{rotD}), the rotational added mass moment coefficient (C_{rotAM}), the chord length of the body (L_z) and the density of water (ρ) [46]. No standard equations are known for resistance against rotation as is the case for resistance against translation. However, when Reynold numbers are not too small, it is common practice to use the approximation that terms of drag are proportional to angular velocity ($\dot{\varphi}(t)$) squared (with drag always opposing the direction of motion, hence best written as $\propto -|\dot{\varphi}(t)|\dot{\varphi}(t)$) [39,40,44,47]. Furthermore, in aquatic environments, added mass is an important term in the resistance against roll, as the density of the body and the surrounding media is similar so that the added mass is not negligible. Added mass is the effect of the inertial forces exerted by the surrounding fluid on an accelerating (or decelerating) body. The moment that is required to accelerate the added mass is proportional to the angular acceleration ($\ddot{\varphi}(t)$) of the body [46,48]. To make the rotational drag coefficient and the rotational added mass moment coefficient dimensionless, a factor of length to the fifth power was added. We chose the chord length of the body (L_z) to the fifth power as this normalization factor to account for the dimensions of the body [46]. These coefficients are useful for assessing the change in rotational drag and rotational added mass of the carapace due to keel reduction, independently of instantaneous acceleration and velocity.

To separate the drag and added mass components from the $M_z(t)$ output from the CFD, for each simulation, a quadratic equation was fitted to the time-dependent moment function using Matlab (The MathWorks Inc., Natick, USA) to determine the rotational drag moment coefficient and the rotational added mass moment coefficient. Since the coefficients were independent of the acceleration experienced by the body, the arithmetic mean was calculated from the three results obtained with the three accelerations.

2.8. Statistics

Our main goal was to qualitatively evaluate the magnitude and direction of the hydrodynamic difference between the original carapace model and the carapace model with reduced keels for each species; and to assess whether the effects are consistent among the different species. Additionally, to evaluate the generality of the effects of the keel-reducing treatment for boxfish as a group, we performed paired Student's *t*-tests ($N = 5$ species). To pass the normality test (Shapiro–Wilk), drag coefficient data were $\log_{10}$-transformed. One-tailed test results are reported because of the directional prediction of the hypotheses, unless the mean direction of the effect is opposite to the prediction. In the latter case, two-tailed test results were performed. Note, however, that these statistical results should be interpreted with care, as species were not entirely randomly selected but rather selected to maximize carapace shape diversity, and the strength of the keel-reducing treatment inevitably differed slightly between species as well (figure 1).

3. Results

3.1. Drag forces and coefficients (H1)

According to the drag hypothesis, a function of the keels would be drag reduction. However, the effect of removing the keels on the drag force and drag coefficient was generally small; in most cases, the keels increased (rather than decreased) the drag force, and the direction of the effect on the drag coefficient (increase or decrease) was not consistent (table 1). Except for *L. triqueter*, the original models experienced a larger drag force than the reduced-keel models (table 1). However, the differences were relatively small, usually less than 4%. The difference was largest in *R. rhinorhynchus*, despite the shape differences between the original model (i.e. original scan) and the reduced-keel model being the smallest, both absolute as relative to its body size (figure 1). For *A. guineensis*, *L. triqueter* and *O. cubicus*, the drag coefficient of the original model was smaller than that of the reduced-keel model, which means that the presence of keels slightly decreased the drag coefficient in these species. *L. cornuta* and *R. rhinorhynchus*, however, showed a difference in the opposite sense. The differences in drag coefficient were

Table 1. Drag forces and coefficients at a zero angle of attack in 0.5 m s^{-1} water flow.

	drag force F_D (N)			drag coefficient C_D		
	original model	reduced-keel model	percentage difference[a] (%)	original model	reduced-keel model	percentage difference[a] (%)
A. guineensis	0.0431	0.0415	−3.72	0.127	0.131	2.65
L. triqueter	0.0596	0.0599	0.48	0.168	0.172	2.36
L. cornuta	0.0332	0.0323	−2.65	0.168	0.165	−1.92
O. cubicus	0.0600	0.0597	−0.42	0.164	0.167	1.61
R. rhinorhynchus	0.0233	0.0210	−9.94	0.196	0.181	−7.93

[a]Percentage difference = $(x_{\text{reduced-keel}} - x_{\text{original}})/x_{\text{original}}$. This indicates how much the reduced-keel model is larger (positive) or smaller (negative) relative to the original model.

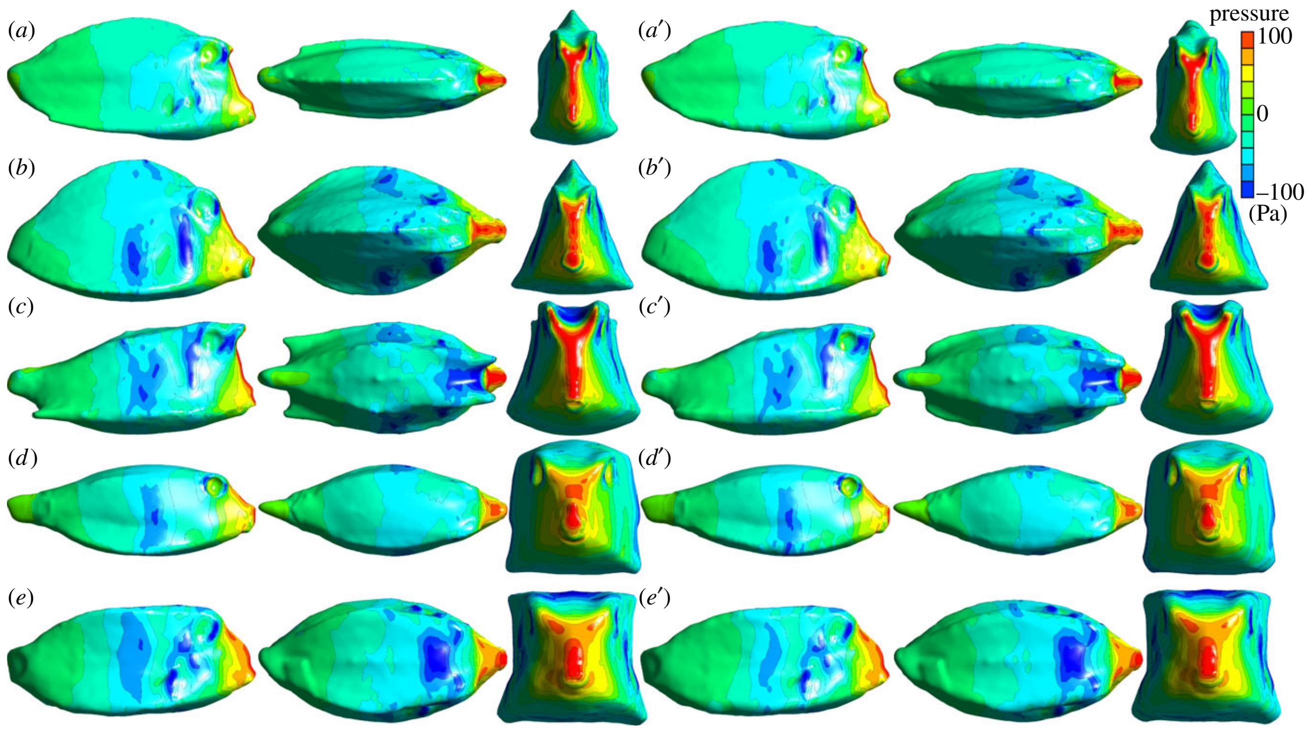

Figure 3. Static pressure experienced by the carapaces with their rostro-caudal axis parallel to a water flow of 0.5 m s^{-1} as calculated by CFD for the original model of (*a*) *A. guineensis*, (*b*) *L. triqueter*, (*c*) *L. cornuta*, (*d*) *O. cubicus* and (*e*) *R. rhinorhynchus*; and (′) their corresponding reduced-keel models. From left to right, views are lateral, dorsal and frontal.

again relatively small (a few per cent, with the exception of *R. rhinorhynchus*) (table 1). As mean differences for the drag force and the drag coefficient were opposite to the prediction of H1, the non-directional null hypothesis that the keels of boxfish do not affect drag was tested, and could not be rejected for both absolute drag forces and drag coefficients (two-tailed paired *t*-test; $p = 0.11$ and $p = 0.82$, respectively).

To obtain a better understanding of the measured drag forces in connection with the presence of keels and the different body shapes, pressure contour plots of the carapace surface were created, as well as 3D iso-surfaces of the vorticity (curl of the velocity field $\nabla \times u$). For all five species, the pressure patterns (figure 3) and 3D iso-vorticity surfaces (electronic supplementary material, figure S1) were almost identical in the original model and the reduced-keel model.

3.2. Pitch moments and coefficients (H2)

The observed pitch moments were positive for all studied species (as defined in figure 2), which suggests that the body would be forced to pitch further away from a horizontal position. The pitch moments about the centre of volume of the carapaces were thus consistently destabilizing (table 2). Overall, the presence of keels made the pitch moment more destabilizing, except in *L. cornuta* and *R. rhinorhynchus*. These differences were relatively small in magnitude; only for *L. cornuta* and *O. cubicus* was the percentage difference larger than 5% (but still maximally 7.5%) (table 2). The pitch moment coefficient, which only conveys the effect of the shape of the carapace—in contrast to the pitch moment, which is also dependent on absolute size and movement speed—was always smaller for the original model than for the reduced-keel model, except for *O. cubicus*. This suggests

Table 2. Pitch moments and coefficients about the centre of volume at a 20° angle of attack in 0.5 m s^{-1} water flow.

	pitch moment M_{pitch} (N m)			pitch moment coefficient C_{Mpitch}		
	original model	reduced-keel model	percentage difference[a] (%)	original model	reduced-keel model	percentage difference[a] (%)
A. guineensis	0.00247	0.00236	−4.38	0.0270	0.0274	1.47
L. triqueter	0.00325	0.00321	−1.16	0.0405	0.0410	1.32
L. cornuta	0.00186	0.00200	7.50	0.0445	0.0519	16.72
O. cubicus	0.00554	0.00518	−6.39	0.0483	0.0461	−4.47
R. rhinorhynchus	0.000898	0.000904	0.70	0.0559	0.0571	2.04

[a]Percentage difference = $(x_{\text{reduced-keel}} - x_{\text{original}})/x_{\text{original}}$. This indicates how much the magnitude of the reduced-keel model is larger (positive) or smaller (negative) relative to the original model.

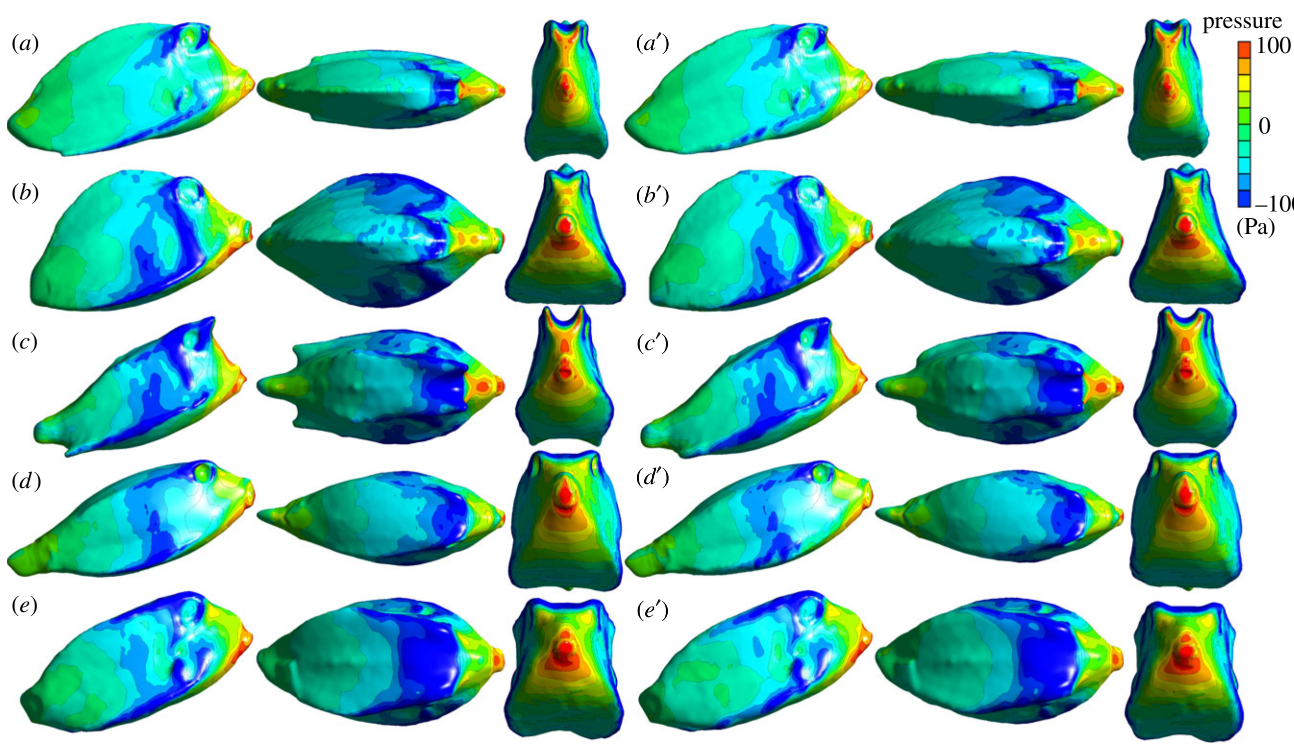

Figure 4. Static pressure on the carapaces at a 20° pitch angle of attack in a water flow of 0.5 m s^{-1} as calculated by CFD for the original model of (*a*) *A. guineensis*, (*b*) *L. triqueter*, (*c*) *L. cornuta*, (*d*) *O. cubicus* and (*e*) *R. rhinorhynchus*; and (′) their corresponding reduced-keel models. From left to right, views are lateral, dorsal and frontal.

that after correcting for size differences between the models, the carapace shape was slightly less destabilizing in pitch for these species when keels were present. The pitch moment coefficient in *L. cornuta* was relatively high compared to those of the other species. In the absence of keels, the pitch moment coefficient was 16.7% larger, that is, 16.7% more destabilizing without keels for *L. cornuta* (table 2). As mean differences for the induced pitch moment were opposite to the prediction of H2, for the absolute pitch moments, instead of the original directional null hypothesis, the null hypothesis that the keels of boxfish do not affect pitch stability was tested and could not be rejected (two-tailed paired t-test; $p = 0.43$). The null hypothesis that the keels of boxfish do not increase pitch stability could not be rejected for pitch moment coefficients (one-tailed paired t-test; $p = 0.21$).

No clear difference could be noted in the pressure patterns (figure 4) and vorticity (electronic supplementary material, figure S1) between the original model and the reduced-keel model under a 20° pitch angle of attack. With the snout rotated up, the ventral region of the snout breaks the water flow, causing a high-pressure area beneath the snout and centred between the eyes and mouth. Negative high-pressure areas were present over the length of the ventral keels, dorsally between the eyes and for some species centrally on the flanks.

3.3. Yaw moments and coefficients (H2)

The observed yaw moment (around the ventral-to-dorsal axis through the centre of volume) was negative for all studied species, which indicates that the body experienced a force to rotate further away from a position in which the rostro-caudal axis was parallel to the water flow. Thus, the yaw moments were consistently destabilizing (table 3). Except for *L. triqueter*, the yaw moments for the original models were more strongly destabilizing, indicating that the presence of

Table 3. Yaw moments and coefficients about the centre of volume at a −20° angle of attack in 0.5 m s^{-1} water flow.

	yaw moment M_{yaw} (N m)			yaw moment coefficient C_{Myaw}		
	original model	reduced-keel model	percentage difference[a] (%)	original model	reduced-keel model	percentage difference[a] (%)
A. guineensis	−0.00976	−0.00974	−0.20	−0.0730	−0.0739	1.21
L. triqueter	−0.00597	−0.00607	1.74	−0.0644	−0.0667	3.61
L. cornuta	−0.00236	−0.00236	−0.10	−0.0572	−0.0584	1.98
O. cubicus	−0.00699	−0.00691	−1.13	−0.0565	−0.0562	−0.59
R. rhinorhynchus	−0.000836	-0.000825	−1.21	−0.0592	−0.0589	−0.58

[a]Percentage difference = $(x_{\text{reduced-keel}} - x_{\text{original}})/x_{\text{original}}$. This indicates how much the magnitude of the reduced-keel model is larger (positive) or smaller (negative) relative to the original model.

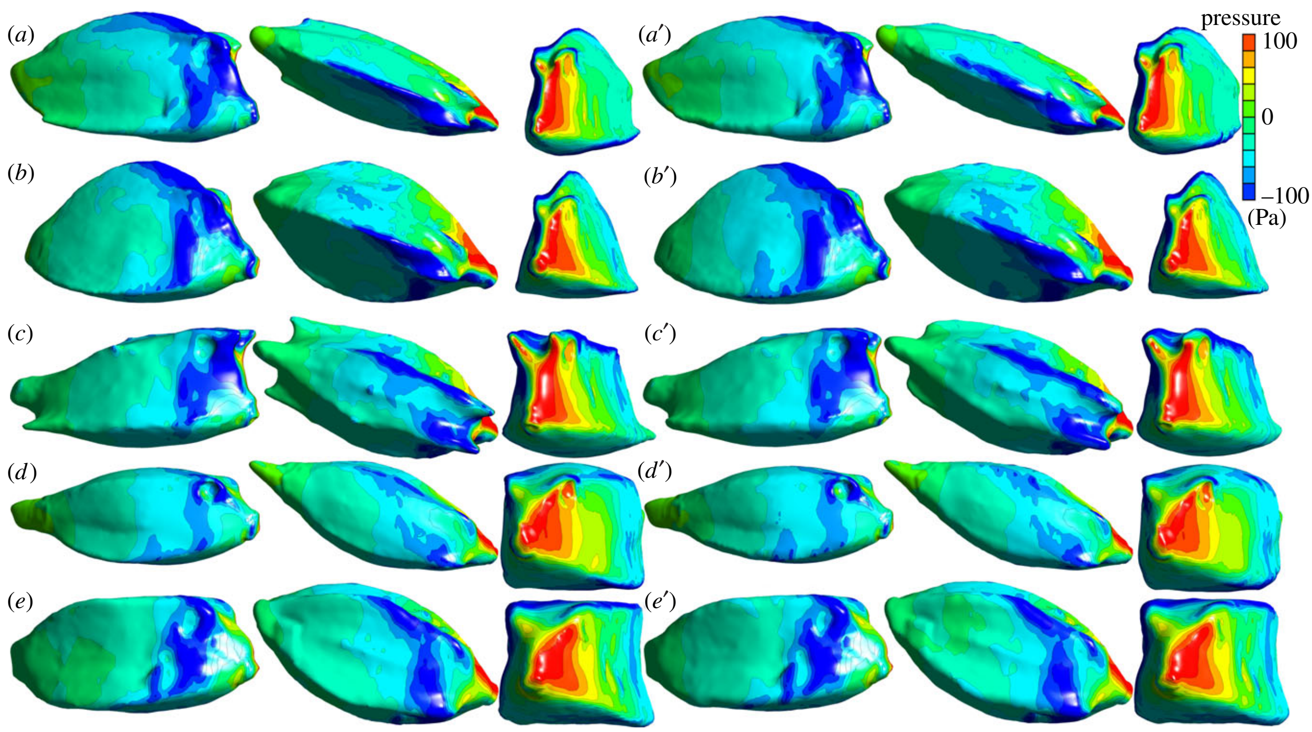

Figure 5. Static pressure experienced by the carapaces at a −20° yaw angle of attack in a water flow of 0.5 m s^{-1} as calculated by CFD for the original model of (*a*) *A. guineensis*, (*b*) *L. triqueter*, (*c*) *L. cornuta*, (*d*) *O. cubicus* and (*e*) *R. rhinorhynchus*; and (′) their corresponding reduced-keel models. From left to right, views are lateral, dorsal and frontal.

keels lowers stability (table 3). However, the differences were always relatively small: less than 2% for each species. In comparing the yaw moment coefficients, except for *O. cubicus* and *R. rhinorhynchus*, the yaw moment coefficients of the original models were lower than those of the reduced-keel models (table 3). The coefficient was slightly less destabilizing for these species when keels were present; however, the differences were very small (smaller than 4%). As mean differences for the induced yaw moments were opposite to the prediction of H2, for the absolute yaw moments, the null hypothesis that the keels of boxfish do not affect yaw stability was tested, and could not be rejected (two-tailed paired *t*-test; $p = 0.94$). The null hypothesis that the keels of boxfish do not increase yaw stability could not be rejected for pitch moment coefficients (one-tailed paired *t*-test; $p = 0.098$).

The pressure patterns on the carapace of the boxfish at yaw angles of −20° showed only subtle differences between the original models and the reduced-keel models (figure 5). As the left side was exposed to the current, high-pressure areas were present from the mouth up to the left eye. Furthermore, there was a strong negative pressure area situated on the right side of the head and over the length of the (left) dorsal keel.

3.4. Resistance against an imposed roll rotation (H3)

The observed rotational drag moment coefficients for roll were all positive. Such positive values indicate that the imposed roll rotation experienced resistance from the hydrodynamic forces on the carapace. The rotational drag moment coefficient was larger for the original model than for the

Table 4. Rotational drag moment coefficient C_{rotD} and rotational added mass moment coefficient C_{rotAM} of the boxfish carapace for imposed roll rotation. Values are means and standard deviation for simulations at three constant accelerations.

	rotational drag moment coefficient C_{rotD}			rotational added mass moment coefficient C_{rotAM}		
	original model (10^{-5})	reduced-keel model (10^{-5})	percentage difference[a] (%)	original model (10^{-5})	reduced-keel model (10^{-5})	percentage difference[a] (%)
A. guineensis	49.6 ± 5.3	23.9 ± 1.2	−51.84	49.0 ± 3.2	40.4 ± 1.8	−17.53
L. triqueter	179 ± 20	110 ± 16	−38.90	115.7 ± 9.3	101.4 ± 9.3	−12.33
L. cornuta	45.5 ± 2.2	30.9 ± 4.1	−32.07	47.7 ± 2.2	41.3 ± 1.2	−13.45
O. cubicus	20.24 ± 0.81	9.6 ± 1.7	−52.43	16.6 ± 1.3	11.74 ± 0.38	−29.44
R. rhinorhynchus	127.8 ± 6.2	79.4 ± 5.3	−37.87	94.2 ± 7.0	82.1 ± 4.4	−12.85

[a]Percentage difference = $(x_{reduced\text{-}keel} - x_{original})/x_{original}$. This indicates how much the magnitude of the reduced-keel model is larger (positive) or smaller (negative) relative to the original model.

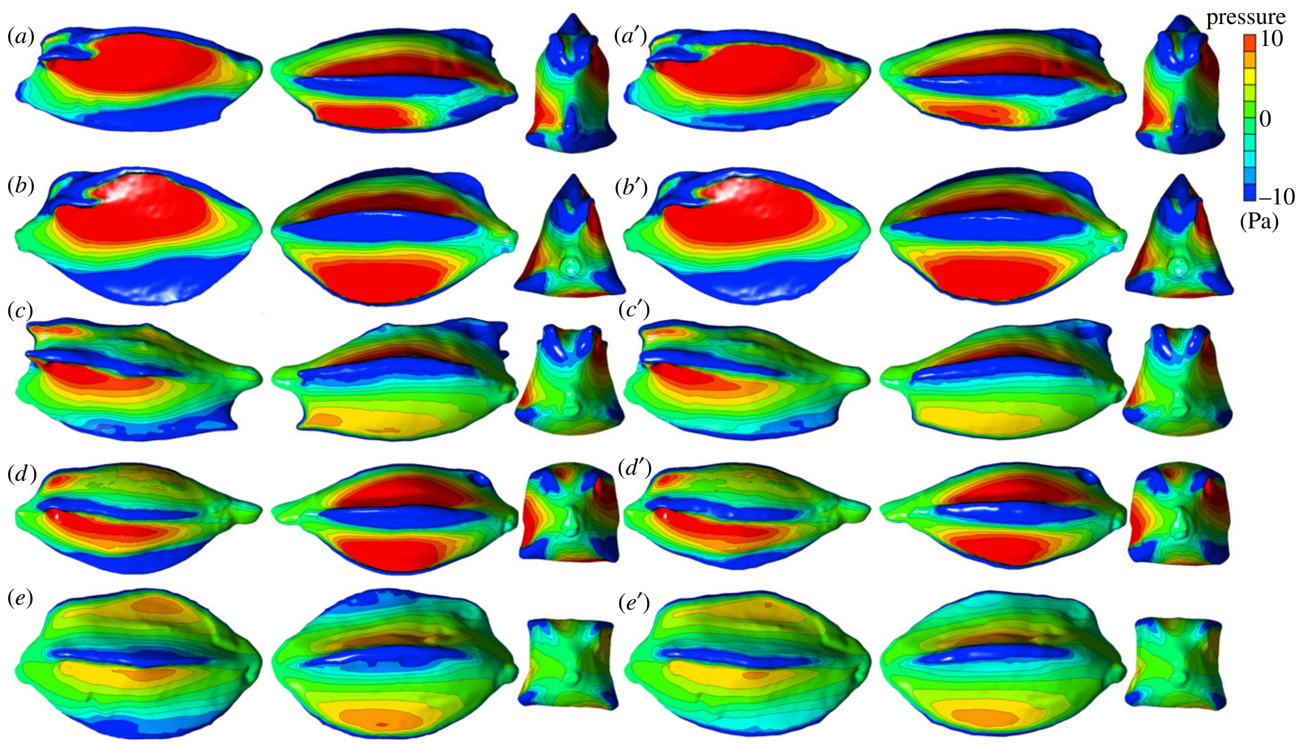

Figure 6. Static pressure experienced by the body while undergoing an imposed roll rotation of constant angular acceleration $\ddot{\varphi} = 40$ rad s^{-2} for $\Delta t = 0.2$ s as calculated by CFD for the original model of (*a*) *A. guineensis*, (*b*) *L. triqueter*, (*c*) *L. cornuta*, (*d*) *O. cubicus* and (*e*) *R. rhinorhynchus*; and (′) their corresponding reduced-keel models. From left to right, views are lateral on the leading side, dorsal with the leading side at the top and trailing side at the bottom and frontal (clockwise rotation in this view).

reduced-keel model in all studied species (table 4). For *A. guineensis* and *O. cubicus*, the rotational drag coefficient for the original model was twice as large as for the reduced-keel model: the absence of keels resulted in a reduction of the coefficient with 51.8% and 52.4%, respectively. For the other species, the percentage difference lay between 30% and 40%. The rotational added mass moment coefficient was also consistently larger for the original model than for the reduced-keel model for all studied species (table 4). The rotational added mass moment coefficient was between 10% and 30% lower in the reduced-keel carapaces, depending on the species. The null hypothesis that the keels of boxfish do not increase resistance against roll was rejected for both roll rotational drag moment coefficients (one-tailed paired *t*-test; $p = 0.019$) and roll rotational added mass moment coefficients (one-tailed paired *t*-test; $p = 0.0031$). Thus, the keels significantly increased the body's resistance to imposed roll rotations through both drag and added mass effects. This should not be confused with roll stability, which was not studied here; this result specifically demonstrates that a boxfish body that possesses keels will be brought out of balance less quickly.

High-pressure areas were present on the side of the keels to which the body rotated, as this side had to push aside the water (figure 6). Negative pressure areas were created at the rear end of the keels. Both of these pressures counteracted the rotation at the two sides of the keels. High-pressure areas, but especially the negative high-pressure areas, were larger in the original model than in the reduced-keel model.

4. Discussion

The goal of this study was to test three hypotheses regarding the potential hydrodynamic functions of the keels on the carapaces of boxfish proposed in the literature. This was achieved by quantifying how strongly the performance of the carapace shapes with normal keels differed compared to the modified carapace shapes, in which the size of the keels was reduced (figure 1). The results of our CFD analysis (tables 1–4), also summarized in electronic supplementary material, figure S2, show that only one of the evaluated hydrodynamic quantities benefits strongly, and consistently among the five species, from the extending, sharp shape of the keels: an increased resistance against rolling. A few millimetres of rounding and flattening of the keels (figure 1) resulted in significant roll drag increases between 32% and 52% (table 4).

These results firmly suggest a functional resemblance to ship keels. The resistance of the carapace to roll, which can be induced by external torques originating from its own fin movements or from water currents onto the body, could be an important factor in the dynamic stability of boxfish. A first contributing factor to rotational stability is inertia. The mass of the body, or more precisely, the mass moment of inertia about the roll axis, is an important part of inertia, although not specifically addressed in this study. However, our data show that the keels notably increased the inertial resistance against rolling by increasing the added mass effect by the surrounding water (i.e. acceleration reaction) for roll by between 12% and 30%. As the definition of inertia indicates, such increased rotational inertia opposes roll acceleration, which is useful because less kinetic energy is built up for a given perturbation impulse. However, once a certain roll velocity has been built up, higher inertia will have an adverse effect and will impede the halting of an undesired roll motion. Therefore, the non-inertial factors of resistance, in our study included jointly into the roll drag coefficient C_{rotD} (table 4 and electronic supplementary material, figure S2) are probably more important, as they will dampen roll perturbations by dissipating roll energy. Moreover, the results showed that the increase in rotational drag due to the keels (32–52%) was consistently higher than the increase they caused in the rotational added mass. Damping of roll motions is also the main function of keels in boats [49].

Studies on swimming in live boxfish seem to confirm their high resistance against roll. Hove *et al*. [11] did not observe any notable roll rotations during straight swimming in *Ostracion meleagris*, whereas low levels of yaw and pitch rotation were observed. This suggests that stabilization against roll rotation is at play. The source of these roll stabilizations could be hydrodynamic, as investigated here, but may also result from hydrostatic (or buoyancy) effects. However, since the centre of mass of boxfish lies at approximately the same height as the centre of buoyancy [11], it is unlikely that gravity and hydrostatic lift cause strong torques to keep the midsagittal plane vertically and thereby resist roll. Therefore, we hypothesize that hydrodynamic damping of roll rotations is the main factor contributing to dynamic roll stability in boxfish.

Other properties of the carapace shape of boxfish may also contribute to roll stability. In our study, only the influence of the edges of the keels was analysed. The square or triangular cross-section of many ostraciid species will be superior in roll damping compared to more cylindrical shapes. The concaveness of large parts of the surfaces of the carapace of boxfish [23], which indirectly form the keels, may aid in roll stability as well. The anal fin may also play a role in this process. Further research is required to evaluate the contribution of these anatomical characteristics to roll damping.

Several morphological and behavioural traits may call for additional structures to aid in roll stabilization in boxfish, that are different in other fishes. Unlike many fishes, boxfish do not have pelvic fins or sturdy, elongated median fins that can be erected to passively dampen roll torques by enlarging the surface area [50,51]. As pectoral fin movement is one of the main drivers of their manoeuvres, these fins cannot be engaged as passive stabilizers at the same time. Moreover, Their relatively wide body, due to the carapace, implies that the pectoral fins are relatively distant from the roll axis. This increases the potential to produce undesired roll torques during swimming and manoeuvring. A laterally compressed body shape with a large body depth, which is common in shallow water reef fish [52], has a higher roll resistance than the boxy shapes of Ostraciidae. For these reasons, the adaptive value of keel-like structures on the body may be higher in boxfish than in other aquatic animals that have different morphology and swimming styles.

By contrast to the consistent increase in resistance against roll that was observed (H3), no evidence was found that keels contribute to drag reduction (H1), or to stability by the generation of stabilizing yaw or pitch torques (H2). First, drag forces were generally lower for the reduced-keel models with digitally reduced keels (table 1). As selective pressures to reduce drag are assumed to be weak because of the relatively slow-moving, non-migratory lifestyle of boxfish, morphological adaptations to reduce drag are unlikely to have evolved [24]. Second, the effect of the keels on the overall pitch and yaw torques exerted by the water on the carapace, when placed at a small angle of attack with respect to the water (figure 2*b*), was generally small, and the direction of the effect varied between species (tables 2 and 3 and electronic supplementary material, figure S2). This indicates that the keels have no function in increasing or decreasing the pitch or yaw stability of the body. Moreover, with regard to the instability of the boxfish body for pitch and yaw, overall destabilizing torques about the centre of volume of the carapace are now confirmed for three more species in addition to the two species that were previously studied [24]. As mentioned in the introduction, the absence of stabilizing effects of the keels on yaw and pitch could be expected, as this would be in line with the ecological demands of the boxfish to maintain sufficient manoeuvrability and agility [10,12]. To manage yaw and pitch, boxfish seem to rely on active control by the fins to tune their level of stability or manoeuvrability according to the circumstances [13].

5. Conclusion

Our study has shed new light on several hypotheses on hydrodynamic functions that were previously attributed to the presence of keels on the carapace of boxfish. Computational modelling simulations on the effects of reducing the keels showed that keels have no drag-reducing effect and do not contribute to passive stability for pitch and yaw rotations, but they significantly increase the damping of roll. These results open up new avenues of research on how this improved roll damping and roll-added mass by the keels could contribute to swimming and manoeuvring performance. This knowledge can, in turn, be used to enhance roll stability in autonomous underwater vehicles without undermining manoeuvrability.

Ethics. For the five covered species, models were obtained by laser scanning museum specimens. Specimen number and the institution holding it for each species: *Acanthostracion guineensis* (accession no. ANSP 102873; Academy of Natural Sciences of Drexel University). *Lactophrys triqueter* (accession no. LACM 8088; Natural History Museum of Los Angeles County). *Lactoria cornuta* (accession no. LACM 38229; Natural History Museum of Los Angeles County). *Ostracion cubicus* (accession no. LACM 42481; Natural History Museum of Los Angeles County). *Rhynchostracion rhinorhynchus* (accession no. SU 28102; former Stanford University collection, now housed in California Academy of Sciences).

Data accessibility. Raw simulation data supporting the findings of this study are available from the Dryad Digital Repository: https://doi.org/10.5061/dryad.qz612jmhh [53].

Supplementary figures are provided in the electronic supplementary material [54].

Authors' contributions. M.J.W.V.G.: formal analysis, visualization, writing—original draft, writing—review and editing; J.G.: methodology, writing—review and editing; M.E.A.: conceptualization, funding acquisition, resources, writing—review and editing; S.V.W.: conceptualization, funding acquisition, resources, writing—original draft, writing—review and editing.

All authors gave final approval for publication and agreed to be held accountable for the work performed therein.

Conflict of interest declaration. We declare we have no competing interests.

Funding. This work was supported by grants from the University of Antwerp (BOF/KP 24346 to S.V.W.), from the Fonds Wetenschappelijk Onderzoek—Vlaanderen (grant no. 1.5.040.18N to J.G.), from the Agence National de la Recherche (grant no. ANR-16-ACHN-0006-01 to S.V.W.) and by the NSF (grant no. DEB 0842397 to M.E.A.).

Acknowledgements. We thank Tina Marcroft for help with laser scanning.

References

1. Weihs D. 2002 Stability versus maneuverability in aquatic locomotion. *Integr. Comp. Biol.* **42**, 127–134. (doi:10.1093/icb/42.1.127)
2. Webb PW. 2002 Control of posture, depth, and swimming trajectories of fishes. *Integr. Comp. Biol.* **42**, 94–101. (doi:10.1093/icb/42.1.94)
3. Weihs D. 1993 Stability of aquatic animal locomotion. *Contemp. Math.* **141**, 443–461. (doi:10.1090/conm/141/19)
4. Webb PW. 2000 Maneuverability versus stability? Do fish perform well in both? In *1st Int. Symp. Aqua Bio-mech./Int. Semin. Aqua Bio-mech., Honolulu, HI, 27–30 August*, pp. 21–29. Tottori, Japan: Society of Aero Aqua Bio-mechanics.
5. Bang K, Kim J, Lee SI, Choi H. 2016 Hydrodynamic role of longitudinal dorsal ridges in a leatherback turtle swimming. *Sci. Rep.* **6**, 1–10. (doi:10.1038/srep34283)
6. Meunier FJ, Francillonviellot H. 1995 Structure and mineralization of the scutes in *Ostracion lentiginosum* (Teleostei, Tetraodontiforme, Ostraciidae). *Ann. Sci. Nat. Zool. Biol. Anim.* **16**, 33–46.
7. Besseau L, Bouligand Y. 1998 The twisted collagen network of the box-fish scutes. *Tissue Cell* **30**, 251–260. (doi:10.1016/S0040-8166(98)80073-6)
8. Yang W, Naleway SE, Porter MM, Meyers MA, McKittrick J. 2015 The armored carapace of the boxfish. *Acta Biomater.* **23**, 1–10. (doi:10.1016/j.actbio.2015.05.024)
9. Vermeij GJ. 1987 *Evolution and escalation: an ecological history of life*. Princeton, NJ: Princeton University Press.
10. Blake RW. 1977 On ostraciiform locomotion. *J. Mar. Biol. Assoc. UK* **57**, 1047–1055. (doi:10.1017/S0025315400026114)
11. Hove JR, O'Bryan LM, Gordon MS, Webb PW, Weihs D. 2001 Boxfishes (Teleostei: Ostraciidae) as a model system for fishes swimming with many fins: kinematics. *J. Exp. Biol.* **204**, 1459–1471. (doi:10.1242/jeb.204.8.1459)
12. Walker JA. 2000 Does a rigid body limit maveuverability? *J. Exp. Biol.* **203**, 3391–3396. (doi:10.1242/jeb.203.22.3391)
13. Boute PG, Van Wassenbergh S, Stamhuis EJ. 2020 Modulating yaw with an unstable rigid body and a coursestabilizing or steering caudal fin in the yellow boxfish (*Ostracion cubicus*). *R. Soc. Open Sci.* **7**, 200129. (doi:10.1098/rsos.200129)
14. Gordon MS, Hove JR, Webb PW, Weihs D. 2000 Boxfishes as unusually well-controlled autonomous underwater vehicles. *Physiol. Biochem. Zool.* **73**, 663–671. (doi:10.1086/318098)
15. Kodati P, Deng X. 2006 Towards the body shape design of a hydrodynamically stable robotic boxfish. In *Proc. of the 2006 IEEE/RSJ Int. Conf. on Intelligent Robots and Systems, Beijing, China,* 9–15 October, pp. 5412–5417. Piscataway, NJ: IEEE. (doi:10.1109/IROS.2006.282108)
16. Kodati P, Hinkle J, Deng X. 2007 Micro autonomous robotic ostraciiform (MARCO): design and fabrication. In *Proc. 2007 IEEE Int. Conf. on Robotics and Automation, Rome, Italy,* 10–14 April, pp. 960–965. Piscataway, NJ: IEEE. (doi:10.1109/ROBOT.2007.363109)
17. Hanbo D, Wei W, Wenguang L, Guangming X. 2015 Yaw angle control of a boxfish-like robot based on cascade PID control algorithm. In *6th Int. Conf. on Power Electronics Systems and Applications (PESA)*, vol. 53, *Hong Kong, December 15–17*, pp. 21–25. Piscataway, NJ: IEEE. (doi:10.1109/PESA.2015.7398910)
18. Lachat D, Crespi A, Ijspeert AJ. 2006 BoxyBot: a swimming and crawling fish robot controlled by a central pattern generator. In *The First IEEE/RAS-EMBS Int. Conf. on Biomedical Robotics and Biomechatronics, Pisa, Italy, 20–22 February,* pp. 643–648. Piscataway, NJ: IEEE. (doi:10.1109/BIOROB.2006.1639162)

19. Zhang H, Wang W, Qu Y, Wang C, Fan R, Xie G. 2016 Model identification for the yaw motion of a tail-actuated robotic fish. In *Proc. of the 2016 IEEE Int. Conf. on Robotics and Biomimetics (ROBIO), Qingdao, China, 3–7 December*, pp. 313–318. Piscataway, NJ: IEEE. (doi:10.1109/ROBIO.2016.7866341)
20. Kadiyam J, Mohan S. 2019 Conceptual design of a hybrid propulsion underwater robotic vehicle with different propulsion systems for ocean observations. *Ocean Eng.* **182**, 112–125. (doi:10.1016/j.oceaneng.2019.04.069)
21. Bartol IK, Gordon MS, Gharib M, Hove JR, Webb PW, Weihs D. 2002 Flow patterns around the carapaces of rigid-bodied, multi-propulsor boxfishes (Teleostei: Ostraciidae). *Integr. Comp. Biol.* **42**, 971–980. (doi:10.1093/icb/42.5.971)
22. Bartol IK, Gharib M, Weihs D, Webb PW, Hove JR, Gordon MS. 2003 Hydrodynamic stability of swimming in ostraciid fishes: role of the carapace in the smooth trunkfish *Lactophrys triqueter* (Teleostei: Ostraciidae). *J. Exp. Biol.* **206**, 725–744. (doi:10.1242/jeb.00137)
23. Bartol IK, Gharib M, Webb PW, Weihs D, Gordon MS. 2005 Body-induced vortical flows: a common mechanism for self-corrective trimming control in boxfishes. *J. Exp. Biol.* **208**, 327–344. (doi:10.1242/jeb.01356)
24. Van Wassenbergh S, van Manen K, Marcroft TA, Alfaro ME, Stamhuis EJ. 2015 Boxfish swimming paradox resolved: forces by the flow of water around the body promote manoeuvrability. *J. R. Soc. Interface* **12**, 20141146. (doi:10.1098/rsif.2014.1146)
25. Bartol IK, Gordon MS, Webb PW, Weihs D, Gharib M. 2008 Evidence of self-correcting spiral flows in swimming boxfishes. *Bioinspir. Biomim.* **3**, 014001. (doi:10.1088/1748-3182/3/1/014001)
26. Froude W. 1865 On the practical limits of the rolling of a ship in a seaway. *Trans. Inst. Naval Arch.* **6**, 175–184.
27. Bryan GH. 1900 The action of bilge keels. *Trans. R. Inst. Naval Arch.* **42**, 198–239.
28. Martin M. 1958 Roll Damping Due to Bilge Keels. Report prepared by the Iowa University Institute of Hydraulic Research for the Office of Naval Research under Contract No. 1611 (01).
29. Kato H. 1965 Effect of bilge keels on the rolling of ships. *J. Soc. Naval Arch.* **117**, 93–114. (doi:10.2534/JJASNAOE1952.1965.93)
30. Lewis EV. 1988 *Principles of naval architecture, volume I: stability and strength*, second revision. Jersey city, NJ: The society of naval architects and marine engineers.
31. Barrass B, Derrett DR. 2006 *Ship stability for masters and mates*, 6th edn. Amsterdam, The Netherlands: Elsevier.
32. Irkal MAR, Nallayarasu S, Bhattacharyya SK. 2019 Numerical prediction of roll damping of ships with and without bilge keel. *Ocean Eng.* **179**, 226–245. (doi:10.1016/j.oceaneng.2019.03.027)
33. Marzouk OA, Nayfeh AH. 2009 Control of ship roll using passive and active anti-roll tanks. *Ocean Eng.* **36**, 661–671. (doi:10.1016/j.oceaneng.2009.03.005)
34. White AS. 2013 Limits to control of ship capsize using cycloidal propellers compared to active fins. *World J. Model. Simul.* **9**, 130–138.
35. Bassler CC, Reed AM, Brown AJ. 2010 A method to model large amplitude ship roll damping. In *Proc. of the 11th Int. Ship Stability Workshop, Wageningen, The Netherlands, 21–23 June*, pp. 217–224.
36. Miyake T, Ikeda Y. 2013 A study on roll damping of bilge keels for new non-ballast ship with rounder cross section. In *Proc. of the 13th Int. Ship Stability Workshop, Brest, France, 23–26 September*, pp. 36–43.
37. Menter FR. 1994 Two-equation eddy-viscosity turbulence models for engineering applications. *AIAA J.* **32**, 1598–1605. (doi:10.2514/3.12149)
38. Etkin B, Reid LD. 1996 *Dynamics of flight, stability and control*. Hoboken, NJ: John Wiley & Sons.
39. Hoerner SF. 1965 *Fluid-dynamic drag*. Bricktown, NJ: Hoerner Fluid Dynamics.
40. White FM. 1998 *Fluid mechanics*, 4th edn. New York, NY: McGraw-Hill Higher Education.
41. Knight R. 2003 *Physics for scientists and engineers: a strategic approach*, 2nd edn. San Francisco, CA: Pearson Addison-Wesley.
42. Brennen C. 1982 A Review of Added Mass and Fluid Inertial Forces. Port Hueneme, CA: Department of the Navy. See https://resolver.caltech.edu/CaltechAUTHORS:BREncel82.
43. McCormick W. 1995 *Aerodynamics, aeronautics, and flight mechanics*, 2nd edn. Hoboken, NJ: John Wiley & Sons.
44. Falkovich G. 2011 *Fluid mechanics: a short course for physicists*. Cambridge, UK: Cambridge University Press.
45. Newman JN. 1977 *Marine hydrodynamics*. Cambridge, MA: MIT Press.
46. Van Wassenbergh S, Day SW, Hernández LP, Higham TE, Skorczewski T. 2015 Suction power output and the inertial cost of rotating the neurocranium to generate suction in fish. *J. Theor. Biol.* **372**, 159–167. (doi:10.1016/j.jtbi.2015.03.001)
47. Newton I. 1846 *Newton's principia. The mathematical principles of natural philosophy*, (ed. A Motte). New York, NY: Daniel Adee.
48. Biewener AA, Pated SN. 2018 *Animal locomotion*. Oxford, UK: Oxford University Press.
49. San YK, Howe GCC, Chen VLC, Roy S. 2018 Analysis on rolling damping of a conventional boat fitted with T-shaped bilge keels. *MATEC Web Conf.* **202**, 02007. (doi:10.1051/matecconf/201820202007)
50. Webb PW, Weihs D. 2015 Stability versus maneuvering: challenges for stability during swimming by fishes. *Integr. Comp. Biol.* **55**, 753–764. (doi:10.1093/icb/icv053)
51. Fletcher T, Altringham J, Peakall J, Wignall P, Dorrell R. 2014 Hydrodynamics of fossil fishes. *Proc. R. Soc. B* **281**, 20140703. (doi:10.1098/rspb.2014.0703)
52. Licht M. 2009 Is it possible to determine a special fish group by one habitat? A short discussion. *Stud. Geol. Salmant.* **45**, 181–186. (doi:10.1111/j.0954-6820.1928.tb03879.x)
53. Van Gorp MJW, Goyens J, Alfaro ME, Van Wassenbergh S. 2022 Data from: Keels of boxfish carapaces strongly improve stabilisation against roll. Dryad Digital Repository. (doi:10.5061/dryad.qz612jmhh)
54. Van Gorp MJW, Goyens J, Alfaro ME, Van Wassenbergh S. 2022 Keels of boxfish carapaces strongly improve stabilization against roll. Figshare. (https://doi.org/10.6084/m9.figshare.c.5953471)